SCIENTIFIC REPORTS
nature research

OPEN

Differential regulation of microRNA-15a by radiation affects angiogenesis and tumor growth via modulation of acid sphingomyelinase

Shushan Rana[1], Cristina Espinosa-Diez[2], Rebecca Ruhl[2], Namita Chatterjee[2], Clayton Hudson[2], Eugenia Fraile-Bethencourt[2], Anupriya Agarwal[2,3], Sokchea Khou[2], Charles R. Thomas Jr.[1] & Sudarshan Anand[1,2*]

Activation of acid sphingomyelinase (SMPD1) and the generation of ceramide is a critical regulator of apoptosis in response to cellular stress including radiation. Endothelial SMPD1 has been shown to regulate tumor responses to radiation therapy. We show here that the SMPD1 gene is regulated by a microRNA (miR), miR-15a, in endothelial cells (ECs). Standard low dose radiation (2 Gy) upregulates miR-15a and decreases SMPD1 levels. In contrast, high dose radiation (10 Gy and above) decreases miR-15a and increases SMPD1. Ectopic expression of miR-15a decreases both mRNA and protein levels of SMPD1. Mimicking the effects of high dose radiation with a miR-15a inhibitor decreases cell proliferation and increases active Caspase-3 & 7. Mechanistically, inhibition of miR-15a increases inflammatory cytokines, activates caspase-1 inflammasome and increases Gasdermin D, an effector of pyroptosis. Importantly, both systemic and vascular-targeted delivery of miR-15a inhibitor decreases angiogenesis and tumor growth in a CT26 murine colorectal carcinoma model. Taken together, our findings highlight a novel role for miR mediated regulation of SMPD1 during radiation responses and establish proof-of-concept that this pathway can be targeted with a miR inhibitor.

Technological advances such as stereotactic body radiation therapy (SBRT) and stereotactic radiosurgery (SRS)[1–5] have allowed significant improvements in therapeutic radiation dose escalation. These treatment modalities are able to ablate malignant tissue for excellent local control, however not all disease sites can be treated with these modalities due to toxicity concerns[6–10]. Dose escalation does not only augments DNA damage but also involves a vast number of tumor microenvironment (TME) regulators[11]. Within the TME, high dose radiation modulates the adjacent vasculature, stroma, and immune cells to contribute to the ionizing radiation (IR) response [4]. Radiation elicits endothelial cell dysfunction characterized by associated increased permeability, detachment from the underlying basement membrane, and apoptosis[12,13]. At ablative doses, greater than 8 Gy, there is rapid induction of sphingomyelinase-mediated production of ceramide, which triggers rapid onset of endothelial apoptosis[14]. Indeed, it is thought that endothelial apoptosis dictates the radiosensitivity of tumors. IR-mediated cell death combined with a pro-inflammatory state contributes to an immunostimulatory profile leading to further immunogenic cell death (ICD)[15,16]. In this context, we hypothesized that transcriptional programs in the endothelia triggered by different radiation doses dictated the overall tumor response to radiation.

MiRs play an important role in radiation responses of both malignant cells and the TME[17,18]. miRs are endogenous, short non-coding, single-stranded RNA spanning approximately 22 nucleotides. We and others have shown that radiation regulated miRs alter DNA damage repair pathways, pro-survival signaling pathways, cell-cycle

[1]Department of Radiation Medicine, Oregon Health & Science University, 3181 SW Sam Jackson Park Road, Portland, OR, 97239, USA. [2]Department of Cell, Developmental & Cancer Biology, Oregon Health & Science University, 3181 SW Sam Jackson Park Road, Portland, OR, 97239, USA. [3]Division of Hematology and Medical Oncology, Knight Cancer Institute, Oregon Health & Science University, 3181 SW Sam Jackson Park Road, Portland, OR, 97239, USA. *email: anands@ohsu.edu

checkpoint regulation, and apoptosis; functions which radiation therapy exploits for therapeutic gain[19–23]. Our previous work identified a group of miRs regulated in the tumor vasculature in response to radiation[24]. In particular, we have observed that some miRs in ECs are differentially regulated in response to different doses of radiation. We focused further attention on miRs predicted to target SMPD1. We found that miR-15a expressed the greatest magnitude difference between standard and ablative dose radiation with substantially lower miR-15a levels at higher doses. Our studies show that miR-15a targets SMPD1 in ECs and inhibition of miR-15a decreases EC and tumor cell proliferation, enhances cell death and diminishes tumor growth in a mouse CT26 colorectal carcinoma flank tumor model. Vascular-targeted nanoparticle delivery of miR-15a inhibitor is sufficient to both decrease tumor growth and angiogenesis. Consistent with the immunostimulatory role of miR-15a deficiency in autoimmune and infectious settings[25,26], we found miR-15a inhibition increased cell death pathway proteins and caspase-1 activation. In summary, our findings establish a new miR based regulatory pathway that affects SMPD1 and therefore vascular cell death in response to radiation dose. Inhibition of this pathway may mimic features of high dose radiation and therefore offers avenues for the development of targeted therapeutics.

Materials and Methods

Methods have been adapted from our previous publications[24,27–29].

miRNA profiling. RNA was extracted from HUVECs at 6 h post radiation with either 2 Gy or 20 Gy and miRs were profiled using TaqMan TLDA panels for human microRNAs. miRs proposed to target miR-15a as predicted by TargetScan were further analyzed. The average fold change after normalization to a housekeeping RNA, typically RNU48, is depicted.

Cell culture and reagents. HUVECs (Lonza) were cultured in EBM-2 media (Lonza) supplemented with 10% fetal calf serum (Hyclone). CT-26 cells (ATCC) were culture in RPMI media supplement with 10% fetal calf serum and antibiotics. HCT-116 cells (ATCC) were cultured in McCoy's supplemented with 10% Fetal Calf Serum and antibiotics. Cells were tested and found negative for mycoplasma contamination before use in the assays described.

Transfections. Cells were reverse transfected with miR-15a-5p mimics, inhibitors and their respective controls using Lipofectamine RNAiMAX (Invitrogen) according to manufacturer's instructions. miR mimics and inhibitors were purchased from Life Technologies or Exiqon.

Irradiation. Cells or mice were irradiated on a Shepherd Cesium-137 irradiator at a rate of approximately 1.34 cGy per minute. In tumor-targeted radiation experiments, mice were restrained in a lead shield (Brain Tree Scientific) to minimize exposure to the non-tumor areas.

Cell titer glo/caspase glo. Cells were transfected in a 6 well plate with miR-15a-5p mimic or inhibitor, and the corresponding controls from Exiqon (Qiagen) as previously described. Cells were transferred to a 96 well plate 16 hours post-transfection (1000 cells/well). In some studies, at 24 h post-transfection the cells were irradiated with 0, 2, or 5 Gy. Cell Titer-Glo and Caspase 3/7 Glo were analyzed at 48 h and 96 h, according to manufacturer's instructions.

Western blot and densitometric analysis. After treatment, cells were washed in phosphate-buffered saline (PBS) and lysed in RIPA buffer (Sigma) supplemented with Complete Protease inhibitor cocktail (ROCHE) and Phosphatase inhibitors cocktail 2 and 3 (Sigma). Lysed cells were harvested by scraping, and proteins were analyzed by Western blot. Equivalent amounts of protein were loaded on a 4–12% gradient SDS-polyacrylamide gel (BioRAD) and transferred for 30 min in a TransBlot turbo (BioRAD) onto Nitrocellulose membranes. Membranes were blocked in 5% milk or 3% BSA and incubated with antibodies as indicated: Anti-SMPD1 (OTI3H7, NBP2-45889, Novus Biologicals, or Clone # 563418, R&D Systems 1:1000, overnight, 4 °C), Gasdermin D (96458, Cell Signaling, 1:1000, overnight, 4 °C), GAPDH (D16H11, Cell Signaling, 1:5,000, 1 h RT), β-actin (Sigma, A5316, 1: 5,000 1 h RT) was used as a housekeeping control for the total levels of protein loaded. Membranes were washed in TBST and incubated with secondary antibodies from Licor Biosciences. Licor antibodies used were goat anti mouse 925–68020 (1:15,000) and goat anti rabbit 925–32211 (1:15,000). Blots were scanned on the Licor Odyssey scanner or Azure scanner according to manufacturer's instructions. Bands were quantified manually using ImageJ to calculate the Integrated Density values of the band of interest and normalizing it to the loading control in the same lane.

Immunohistochemistry. CT26 tumors were harvested in PBS, fixed with 4% PFA for 1 hr at room temperature, and soaked overnight in 30% Sucrose. On the following day, they were PBS washed, embedded in OCT, frozen, and stored at −80 °C until cryosectioning. 10 µm sections were blocked with 10% of normal goat serum in 1x PBS containing 0.5% saponin and 2% BSA for 2 hr at room temperature. Sections were then washed with PBS and incubated overnight with anti-CD31 from BD Biosciences (550274; lot 51627341, at 1:100 dilution) followed by secondary antibody Goat anti-Rat Alexa 546 from Invitrogen (A11081; lot 2045302; at 1:400) for 2 hr at room temperature. Sections were mounted in ProLong™ Gold Antifade Mountant with DAPI (P36931) and stored at 4 °C until imaging with Yokogawa CSU-W1 spinning disk confocal microscope with 20 × 0.45 Plan Fluor objective (Nikon). The images were analyzed with Fiji software. Specifically, 3–5 images from at least 3 mice per each treatment group were combined into a single virtual stack and inverted to generate black image on a white background. Thresholds were set to visualize most of the vessels in each image of the stack. The analyze particle

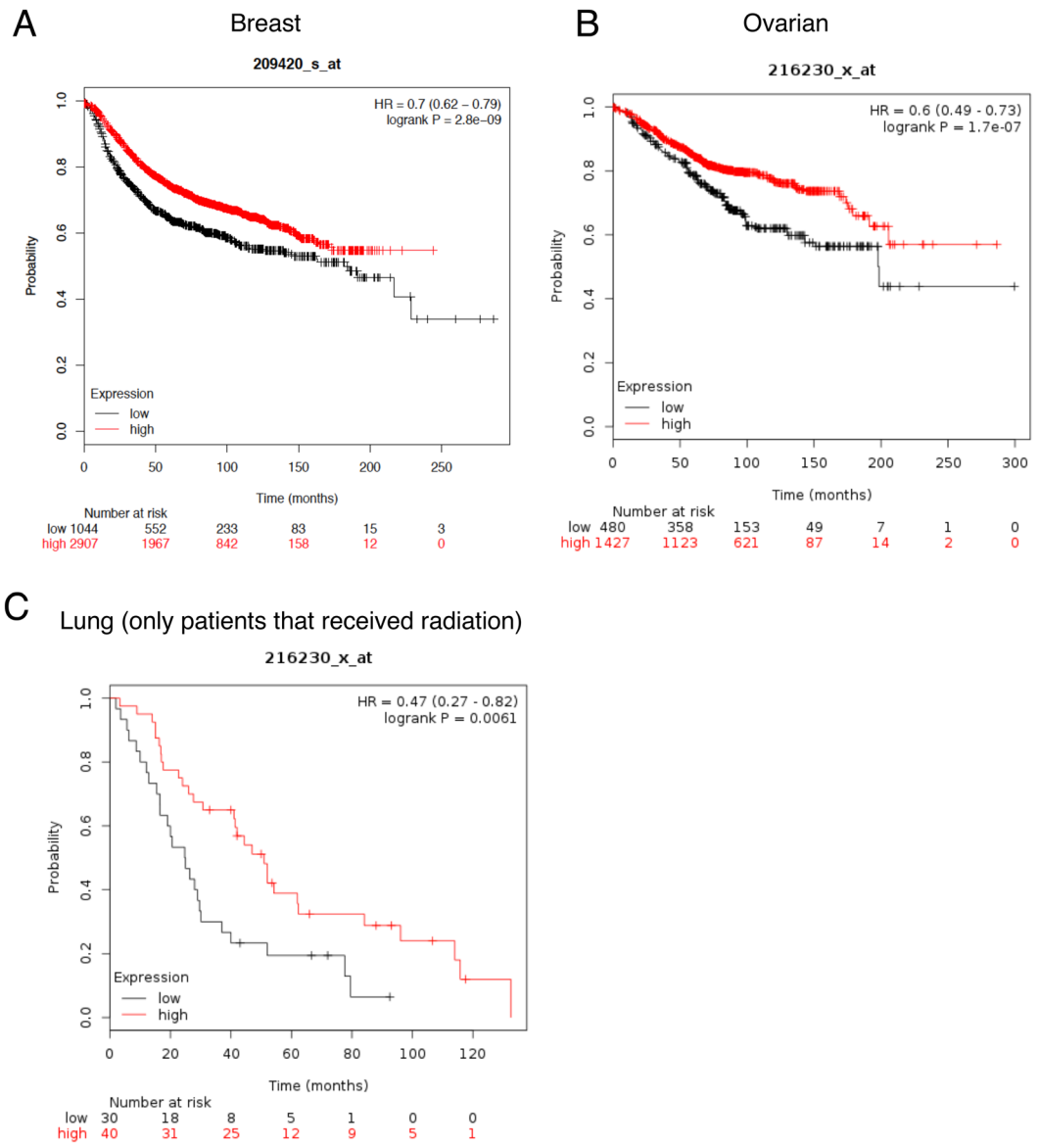

Figure 1. SMPD1 expression correlates with better overall survival in human cancers. Kaplan-Meier plots (kmplotter) showing overall survival in (**A**) Breast, (**B**) Ovarian and (**C**) Lung cancer patients expressing high vs low SMPD1 levels. The expression levels were classified as high or low based on median expression of the gene. The lung cancer dataset was restricted to patients that received radiotherapy.

function with a size limit of 1–25 micron[2] was used to generate both area and density measurements. The area fractions from the CD31 channels were normalized to the area fractions from the DAPI channels.

Multiplex cytokine ELISA. Cytokines were profiled from supernatants from HUVECs at 24 or 72 h post transfection using a 60 cytokine, Human Cytokine/Chemokine Magnetic Bead Panel (Millipore/Sigma HCYTOMAG-60K) kit in a 96 well format per manufacturer's recommendations.

3-D angiogenic sprouting assay. Early passage HUVECs were coated on cytodex-3 beads (GE Healthcare) at a density of 10 million cells/40 μl beads and incubated in suspension for 3–4 hours with gentle mixing every hour. They were plated on TC treated 6 well dishes overnight and resuspended in a 2 mg/ml fibrin gel with 200,000 human smooth muscle cells. The gel was allowed to polymerize and complete EGM-2 media was added. Sprouts were visualized from days 3–4 via confocal imaging after overnight incubation with FITC labeled *Ulex europaeus* lectin (Vector labs). Immunofluorescence imaging was performed on a Yokogawa CSU-W1 spinning disk confocal microscope with 20 0.45 Plan Fluor objective (Nikon).

***In vivo* assays.** All animal work was approved by the OHSU Institutional Animal Use and Care Committee. All experiments were performed in accordance with the relevant guidelines and regulations. 8–10 week old Balb/C mice purchased from Jackson Labs were injected subcutaneously with 5×10^5 tumor cells in Matrigel

A

		Predicted consequential pairing of target region (top) and miRNA (bottom)	Site type	Context++ score
Position 331-337 of SMPD1 3' UTR	5'	...CCAGGAACCCUGUACUGCUGCUG...	7mer-m8	-0.29
hsa-miR-15a-5p	3'	GUGUUUGGUAAUACACGACGAU		
Position 331-337 of SMPD1 3' UTR	5'	...CCAGGAACCCUGUACUGCUGCUG...	7mer-m8	-0.29
hsa-miR-15b-5p	3'	ACAUUUGGUACUACACGACGAU		
Position 331-337 of SMPD1 3' UTR	5'	...CCAGGAACCCUGUACUGCUGCUG...	7mer-m8	-0.28
hsa-miR-497-5p	3'	UGUUUGGUGUCACACGACGAC		
Position 331-337 of SMPD1 3' UTR	5'	...CCAGGAACCCUGUACUGCUGCUG...	7mer-m8	-0.26
hsa-miR-424-5p	3'	AAGUUUUGUACUUAACGACGAC		
Position 331-337 of SMPD1 3' UTR	5'	...CCAGGAACCCUGUACUGCUGCUG...	7mer-m8	-0.26
hsa-miR-6838-5p	3'	UCCUCAGAACGGUGACGACGAA		
Position 331-337 of SMPD1 3' UTR	5'	...CCAGGAACCCUGUACUGCUGCUG...	7mer-m8	-0.26
hsa-miR-16-5p	3'	GCGGUUAUAAAUGCACGACGAU		
Position 331-337 of SMPD1 3' UTR	5'	...CCAGGAACCCUGUACUGCUGCUG...	7mer-m8	-0.25
hsa-miR-195-5p	3'	CGGUUAUAAAGACACGACGAU		

B

	2 Gy	20 Gy
miR-15a	2.13	0.02
miR-15b	0.10	1.51
miR-16	1.16	2.87
miR-195	0.52	7.44

Figure 2. Discovery of SMPD1 targeting miRs that are differentially regulated by radiation. (**A**) TargetScan prediction of miR candidates that harbor binding sites on the 3′ untranslated region of human SMPD1. (**B**) miR candidates targeting SMPD1 exhibit radiation dose-dependent differential expression at 6 h post-IR in HUVECs. Fold changes vs control untreated cells are indicated in colored cells relative to expression of the respective miRNA in non-irradiated samples. Red = increased expression. blue = decreased expression.

(BD) per each flank. Tumor growth was measured with calipers, with volume computed as ½ * Length * Width^2. Mice were randomized into groups once the average tumor volume reached 100 mm^3, approximately 7–10 days after injection. miR inhibitors were delivered i.v. in either PBS or vascular targeted 7C1 nanoparticles every two days from randomization for a total of three doses.

Statistics. All statistical analysis was performed using Excel (Microsoft) or Prism (GraphPad). Two-tailed Student's T-test or ANOVA with post-hoc corrections was used to calculate statistical significance. P values <0.05 were considered significant.

Results

SMPD1 expression correlates with better overall survival in breast, ovaraian and lung cancers. We first evaluated the expression of SMPD1 in human cancers and asked if the levels of SMPD1 correlated with overall survival (Fig. 1) using the online database KMplotter. We observed that in breast and ovarian cancers, SMPD1 high patients had significantly better overall survival. In lung cancer patients, data was available for patients that only received radiation therapy. In this subset, SMPD1 high patients had almost two-fold better overall survival than patients with low SMPD1 (Fig. 1C). Analysis of TCGA revealed that SMPD1 is seldom mutated or amplified suggesting transcriptional and/or post transcriptional mechanisms control the expression of SMPD1.

miRs regulating SMPD1 exhibit differential dose expression. Given that miRs are a major mechanism for post-transcriptional control of gene expression, we sought to identify miRs that specifically targeted SMPD1. TargetScan analysis of the SMPD1 3′ untranslated region identified miR-15 family as putative regulators of SMPD1 (Fig. 2A). We chose to evaluate this using ECs as a model system since they express ~20 fold more SMPD1 than tumor cells. We asked if there was any miR-15a family member that was differentially regulated by

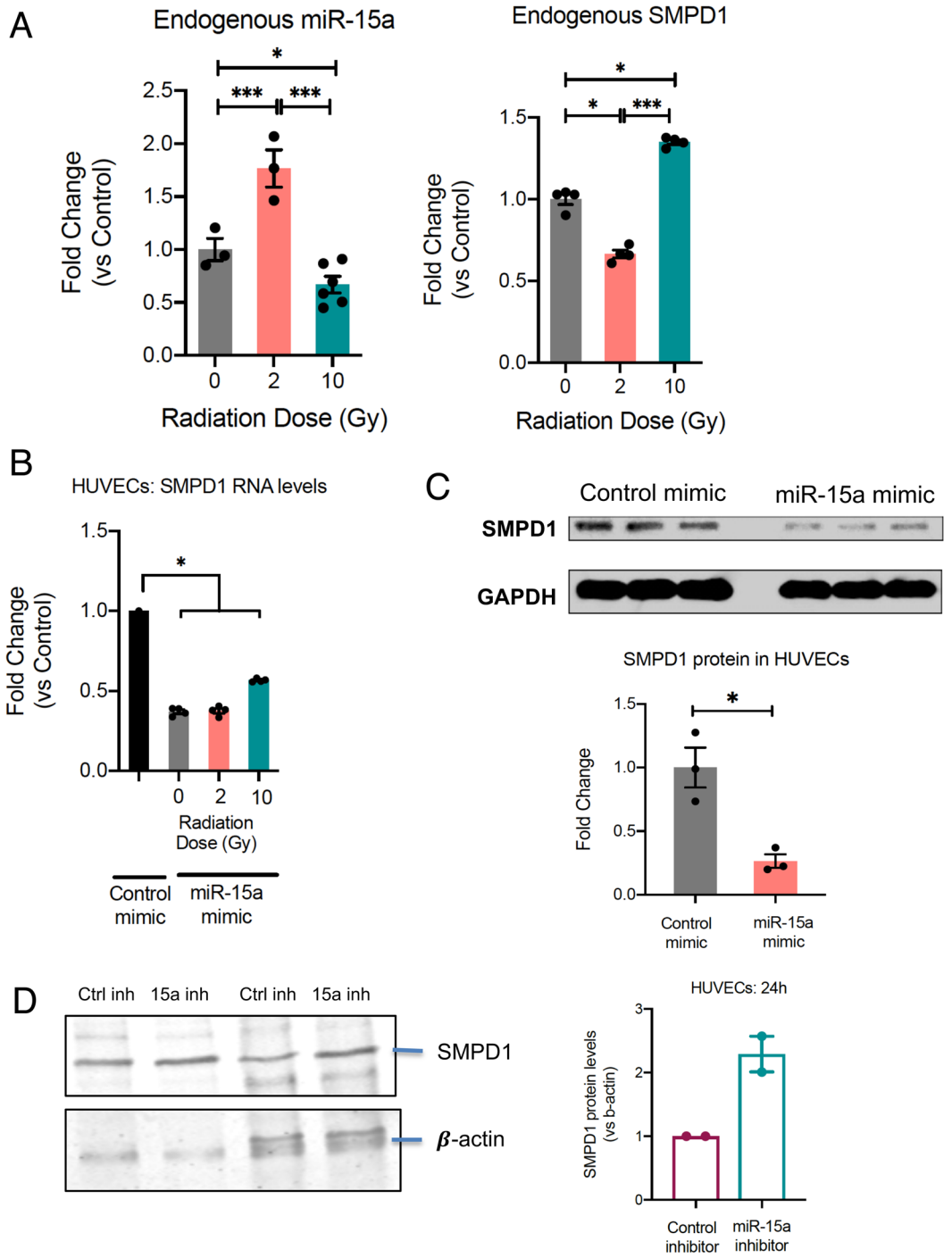

Figure 3. miR 15a decreases SMPD1 expression in endothelial cells. (**A**) Reciprocal regulation of endogenous miR-15a (left) and SMPD1 (right) by high vs low dose radiation. HUVECs were irradiated as indicated and RNA was extracted at 18 h post RT. Bars show mean ± SEM of replicates. (**B**) HUVECs were transfected with either a control mimic or a miR-15a mimic. 24 h later HUVECs were irradiated with the indicated doses. 24 h after radiation, RNA was isolated and qRT-PCR was performed to measure the levels of SMPD1. (**C**) Cells were lysed at 48 h post transfection and SMPD1 protein levels were measured by western blotting. Lanes show biological replicates and bar graph shows mean band intensity ± SEM of replicates. (**D**) SMPD1 protein levels in HUVECs 24 h after transfection. Bars show normalized band intensity ± SEM. *P < 0.05, ***P < 0.001 per ANOVA with post hoc Tukey's test for comparisons between more than 2 groups or two-tailed Student's T-test for two groups.

radiation. HUVECs were treated with either a single 2 Gy or 20 Gy dose via Cs-137 and miRs were profiled at 6 h post treatment. miR-15a exhibited the greatest differential change at 6 hours post-IR between exposure of 2 Gy and 20 Gy radiation relative to non-irradiated samples (Fig. 2B). We first confirmed that endogenous miR-15a decreased at high dose radiation and the expression of SMPD1 was reciprocal to the amount of miR-15a (Fig. 3A)

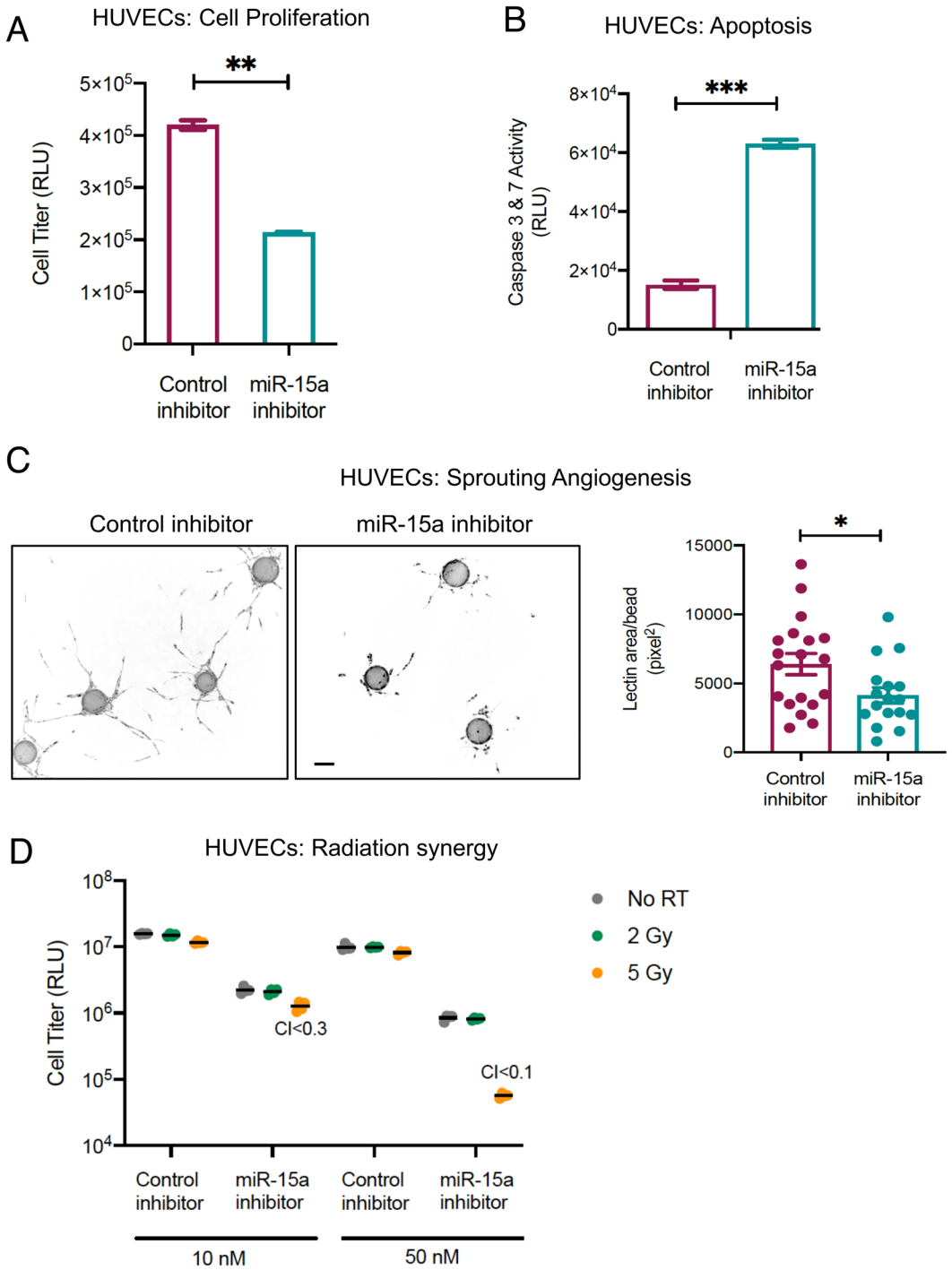

Figure 4. Inhibition of miR-15a decreases endothelial cell proliferation and enhances cell death. (**A**) HUVECs were transfected with either a control negative inhibitor or a miR-15a inhibitor. 48 h later proliferation (**A**) or cell death (**B**) was measured using a luciferase-based Cell Titer glo assay (**A**) or Caspase 3 & 7 CasGlo assay (**B**). (**C**) Fibrin bead 3D angiogenesis assay. HUVECs were transfected as described in A and were coated onto cytodex beads and allowed to sprout in a fibrin gel in the presence of smooth muscle cells over 5 days. The images show representative beads with angiogenic sprouts stained with *Ulex europaeus* lectin for each condition. Bars depict mean +SEM of lectin area analyzed across at least 25 beads per group. Scale bar = 100 μm. D) HUVECs were transfected as described in A with the indicated concentrations of either control inhibitor or miR-15a inhibitor. 24 h later, cells were irradiated at the indicated doses. 48 h post irradiation, proliferation was measured using a Cell Titer glo assay. Synergy was calculated using the Chou-Talalay method with combination index < 1 considered synergistic. Bars indicate means ± SEM of 3 technical replicate wells. One of two independent experiments is shown.

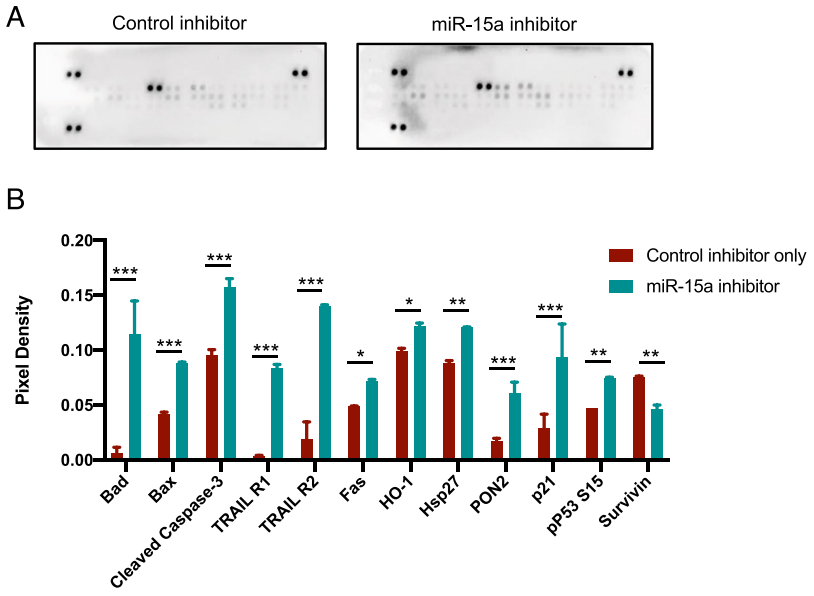

Figure 5. miR-15a inhibition in endothelial cells drives cell death pathways. (**A**) Western blot on a membrane array for human apoptosis pathways (Proteome profiler, R&D Systems). HUVECs were transfected with either control inhibitor or miR-15a inhibitor as described in Fig. 4. 48 h later, cells were lysed and the lysates were incubated with a membrane containing duplicate spots with bound antibodies for different apoptotic proteins and developed with SA-HRP per manufacturer's instructions. (**B**) Densitometry of duplicate spots from the membrane. Bars show mean + SD. Bars are shown only for proteins that were significantly different between the groups via two-tailed Student's T-test followed by a Holms-Sidak post-hoc correction for multiple comparisons (Adjusted *P*-values <0.05). *** denotes adjusted $P < 0.0001$, ** denotes adjusted $P < 0.005$, * denotes adjusted $P < 0.05$.

via qRT-PCR. Subsequently, we confirmed that exogenous transfection of miR-15a increased miR-15a levels in HUVECs (Supplementary Fig. 1), significantly reduced expression of SMPD1 mRNA (Fig. 3B) and protein levels (Fig. 3C, uncropped blot in Supplementary Fig. 2). Our data is consistent with other studies that have also shown that miR-15a targets SMPD1 directly[30]. These observations establish that miR-15a is differentially expressed at low vs high dose radiation and affects SMPD1 levels in ECs.

miR-15a inhibition decreases HUVEC viability and increases caspase activity. Since our data indicates that high dose radiation decreased miR-15a and increased SMPD1, we asked if inhibition of miR-15a affected cell viability. First, we established that miR-15a inhibition with a complementary, chemically stabilized oligonucleotide decreased miR-15a levels (Supplementary Fig. 1) and increased SMPD1 levels (Fig. 3D, uncropped blot Supplementary Fig. 3). HUVECs transfected this with miR-15a inhibitor demonstrated decreased cell proliferation and increased caspase activation (Fig. 4A,B). While noting SMPD1 is characterized by a 20 fold increased expression in ECs relative to other cell types[31], we analyzed the effects of miR-15a inhibitor on malignant cell lines. Similar to HUVECs, miR-15a inhibitor dramatically decreased cell viability in HCT-116 cells and CT26 colorectal carcinoma cells (Supplementary Fig. 4).

We then asked if miR-15a inhibition affected angiogenesis in a physiologically relevant 3D sprouting angiogenesis assay. Consistent with the decreased proliferation and increased cell death, we observed fewer and less robust angiogenic sprouts in miR-15a inhibitor transfected HUVECs (Fig. 4C). Finally, we tested whether miR-15a inhibition synergized with radiation. We observed that in HUVECs, a combination of miR-15a inhibitor and 5 Gy dose of radiation was highly synergistic with a Chou-Talalay combination index less than 0.5 at both 10 and 50 nM doses. These observations indicate that miR-15a inhibition can decrease angiogenesis as well as act in concert with radiation.

We observed that consistent with other reports, miR-15a inhibition affected pro-apoptotic pathways including induction of Bad, TRAIL receptors, p21 and decrease in pro-survival protein Survivin (Fig. 5). We also observed that miR-15a inhibition enhanced inflammasome activation. We found that miR-15a mimic decreased the expression of Gasdermin D a key regulator of pyroptosis[32] while miR-15a inhibition increased Gasdermin D (Supplementary Fig. 5A). In addition, miR-15a inhibitor also increased the activity levels of executioner caspase Caspase-1(Supplementary Fig. 5B). Pyroptosis is a lytic, regulated cell death that requires the enzymatic activity of inflammatory caspases. Since pyroptosis releases intracellular danger associated molecular patterns (DAMPs) and cytokines such as IL-1, it is thought to be a more immunogenic form of cell death[33]. Recent evidence indicates there is significant cross-talk apoptosis and pyroptosis to regulate the inflammatory response[34]. Indeed, we found miR-15a inhibition increased a number of cytokines and chemokines including IL-1, PDGF while significantly downregulating IL-4, 5 and Fractalkine levels (Supplementary Fig. 6).

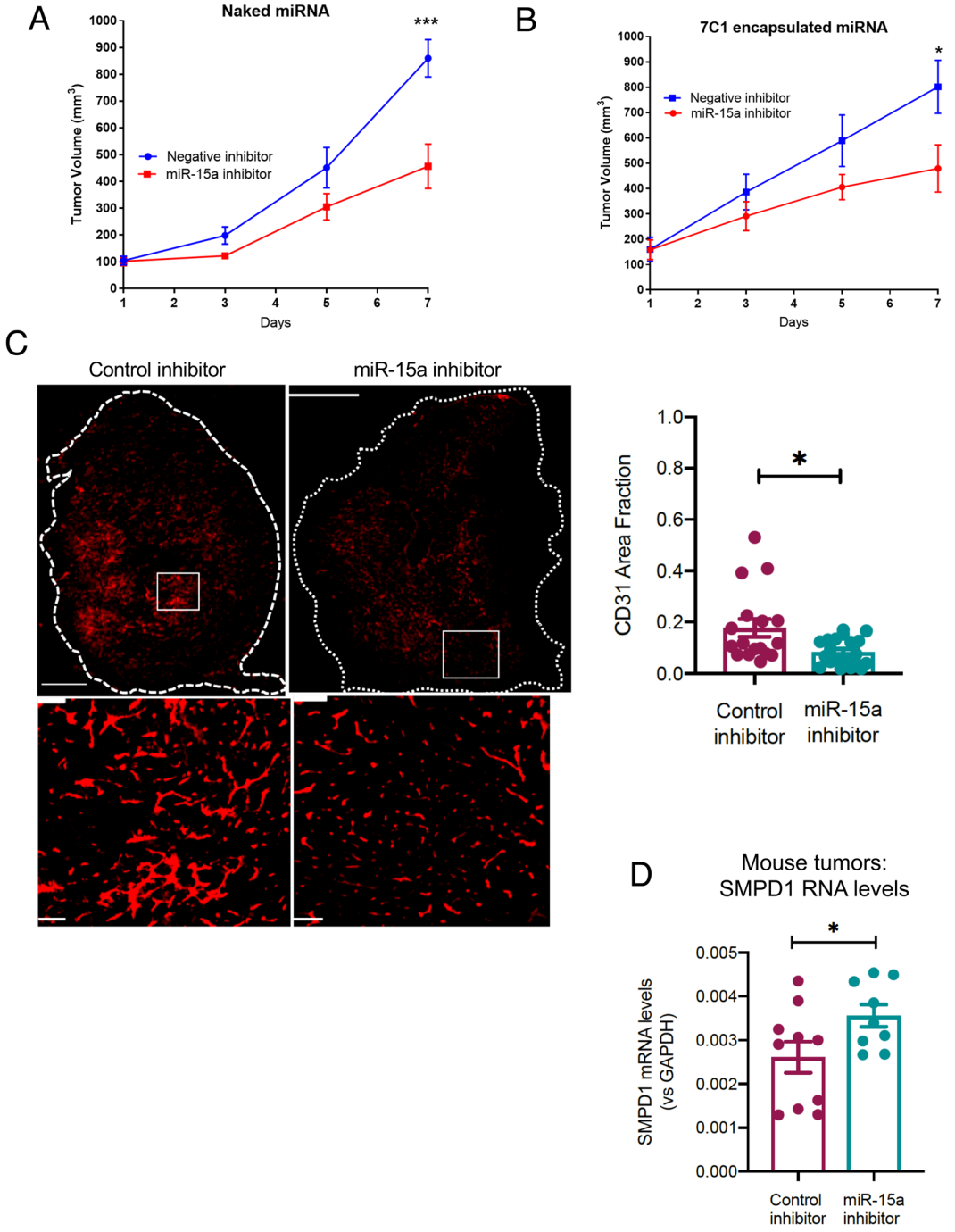

Figure 6. Systemic or vascular inhibition of miR-15a decreases tumor burden. (**A**) CT26 tumors were implanted subcutaneously in Balb/C mice (N = 5 mice per group, two tumors per mouse). Once tumors reached 100 mm^3 volume, mice were randomly assigned to either a negative control inhibitor group or a miR-15a inhibitor (20 mg/kg, i.v. in PBS). Mice were treated every two days for a total of three treatments. ***$P < 0.01$; ANOVA. (**B**) In the same model, mice were randomly assigned to receive either a negative control inhibitor or a miR-15a inhibitor in vascular-targeted 7C1 nanoparticles (1 mg/kg, i.v.). *$P < 0.05$; ANOVA. (**C**) CD31 staining showing blood vessels in the tumors from B). Scale bar = 1000 μm. Dotted line shows whole tumor outline. Bottom panels show a magnified view of the boxed region. Scale bar = 100 μm. Bars show mean + SEM of 3–4 tumor sections from each mouse. Dots represent individual tumor sections. *$P < 0.05$, Mann-Whitney U-test. (**D**) SMPD1 mRNA levels at endpoint measured via qRT-PCR from tumors in B. *$P < 0.05$, Student's T-test.

Inhibition of miR-15a in the vasculature decreases tumor growth and angiogenesis. We next assessed whether miR-15a inhibitor had any effects on tumor growth *in vivo* and if these effects were dependent on its regulation of angiogenesis. In a murine CT26 colorectal carcinoma flank tumor model, systemic treatment with i.v. injected miR-15a inhibitor resulted in an approximately 50% decrease in tumor growth after 7 days (Fig. 6A).

Since our *in vitro* experiments demonstrated miR-15a inhibition also affected CT26 proliferation, it is possible that this tumor delay was a result of direct tumor cell inhibition. To address this, we took advantage of a vascular-targeted nanoparticle that we have established as an efficient platform for delivering miRs to tumor vasculature and not tumor cells. We found that delivery of vascular-targeted miR-15a inhibitor in the same model was sufficient to decrease tumor burden (Fig. 6B). Importantly, the tumors treated with miR-15a inhibitor had a significant decrease in angiogenesis as measured by CD31 area (Fig. 6C). We noted that the tumors treated with miR-15a inhibition in this experiment also had higher levels of SMPD1 mRNA levels (Fig. 6D). Taken together, our observations indicate that miR-15a, a regulator of SMPD1, is inhibited by high dose radiation in ECs. A synthetic miR-15a inhibitor not only decreased EC proliferation *in vitro* but also decreased angiogenesis and tumor growth *in vivo*.

Discussion

The importance of the TME in radiation has been elucidated with the advent of new technologies and techniques allowing safer radiation dose escalation that engages the TME components[11]. Kolesnick *et al*. were among the first to demonstrate the importance of dose magnitude in eliciting rapid endothelial apoptosis via SMPD1 translocation to the plasma membrane. This translocation of SMPD1 produced ceramide thereby facilitating enhanced FAS-FASL and TNFRSF10-TNFLSF10 apoptotic signaling[31]. While earlier pre-clinical models focused attention on single high dose radiation, this is not directly clinically applicable to most disease sites given dose limitations to adjacent critical organs. With this constraint, total radiation dose is divided over several days to allow sublethal damage repair of normal tissue. Using a syngeneic CT26 colorectal cancer model, Zhu *et al*. compared fractionation between 6 Gy × 5 fractions and 12 Gy × 3 fractions. In the 6 Gy cohort, only a cumulative dose of 12 Gy or higher led to incremental increased SMPD1 activity, increased endothelial cell apoptosis, and decreased microvessel density. In contrast, multiple administrations of 12 Gy did not significantly change SMPD1 function or EC apoptosis rates[35].

As radiation dose dictates SMPD1 activity, as well as the expression of distinct miRs, we asked whether miRs with predicted binding to the SMPD1 3′-UTR also exhibited dose dependent differential expression. Interestingly, among our miRNA microarray, there were three miRs targeting SMPD1, which increased with higher doses of radiation. However, just a single miR, miR-15a was increased nearly 2-fold at 2 Gy and decreased significantly with the ablative dose radiation of 20 Gy. Recent insight into vascular miR-15a, elucidates oxidative stress as an inhibitor of miR-15a expression and the subsequent rise in SMPD1 activity. In retinal ECs, Wang *et al*. confirmed that miR-15a binds directly to the 3′-UTR of SMPD1, and also that miR-15a inhibition significantly increases ceramide production. Indeed, miR-15a inhibition has been shown to increase expression of pro-inflammatory cytokines such as IL-6, IL-1β, and TNF-α[30] and increased leukostasis, elevated CD45, and NF-κB levels[36] in different pathophysiological contexts.

In the oncogenic context, miR-15a inhibition has been shown to enhance the innate immune response in favor of anti-tumor immunity. Yang *et al*.[37] found that miR-15a deficiency inhibited tumor growth and prolonged survival in an orthotopic glioma model. In these experiments, they demonstrated miR-15a deficiency led to an influx of CD8+ T cells, decreased expression of inhibitory receptors including PD-1, Tim-3, and LAG-3, and increased inflammatory cytokine production.

Given the heterogeneity of cancer and versatile nature of miRs, miR-15a's role as either an oncogenic miR or a tumor suppressive miR does not lie firmly within one category. Several cancers including non-small cell lung cancer and breast cancer, express lower miR-15a levels. This decrease in the miR has been linked to increased tumor growth and radioresistance that is reversible through miR-15a overexpression[38,39]. In colorectal cancer, a recent analysis of 182 patients found that miR-15a overexpression is associated with a worse 5-year progression free survival and overall survival (68% vs 88%, $p = 0.001$; 60% vs 74%, $p = 0.035$, respectively)[40]. However, the dichotomic behavior is not unique to miR-15a, being a largely an oversimplified classification for this molecule able to regulate multiple targets in a context dependent fashion[41].

We chose to use colorectal cancer as our model for *in vivo* studies given the above findings. However, the primary focus remains the influence of vascular miR-15a on the TME to effect anti-cancer activity. SMPD1 is also a known target of miR-15a, consistent with our findings, and they both exhibit dose dependent reciprocal expression. MiR-15a inhibition decreased cellular viability, increased endothelial caspase activity and enhanced both inflammasome activation and Gasdermin expression. These mechanisms suggest that miR-15a inhibition maybe potent due to its ability to drive pyroptosis in the vasculature, which would be beneficial in a therapeutic context. On the basis of these observations, we propose that inhibition of miR-15a offers a unique approach to suppress tumor growth.

Received: 5 March 2018; Accepted: 17 March 2020;
Published online: 27 March 2020

References

1. Lo, S. S. *et al*. The development of stereotactic body radiotherapy in the past decade: a global perspective. *Future Oncol*, https://doi.org/10.2217/fon.15.220 (2015).
2. Rehman, S., Roach, M. C., Bradley, J. D. & Robinson, C. G. Lung Stereotactic Body Radiation Therapy. *Mo Med* **112**, 361–365 (2015).
3. Song, C. W., Kim, M. S., Cho, L. C., Dusenbery, K. & Sperduto, P. W. Radiobiological basis of SBRT and SRS. *Int J Clin Oncol* **19**, 570–578, https://doi.org/10.1007/s10147-014-0717-z (2014).
4. Timmerman, R. D., Herman, J. & Cho, L. C. Emergence of stereotactic body radiation therapy and its impact on current and future clinical practice. *J Clin Oncol* **32**, 2847–2854, https://doi.org/10.1200/JCO.2014.55.4675 (2014).
5. Yu, J. B. & Sandler, H. M. Stereotactic body radiation therapy: Let's not give up on progress. *Pract Radiat Oncol* **5**, 193–196, https://doi.org/10.1016/j.prro.2014.09.001 (2015).
6. Osmundson, E. C. *et al*. Predictors of toxicity associated with stereotactic body radiation therapy to the central hepatobiliary tract. *Int J Radiat Oncol Biol Phys* **91**, 986–994, https://doi.org/10.1016/j.ijrobp.2014.11.028 (2015).

7. Trakul, N., Koong, A. C. & Chang, D. T. Stereotactic body radiotherapy in the treatment of pancreatic cancer. *Semin Radiat Oncol* **24**, 140–147, https://doi.org/10.1016/j.semradonc.2013.11.008 (2014).
8. Dobbelstein, M. & Sorensen, C. S. Exploiting replicative stress to treat cancer. *Nat Rev Drug Discov* **14**, 405–423, https://doi.org/10.1038/nrd4553 (2015).
9. Schaue, D. & McBride, W. H. Opportunities and challenges of radiotherapy for treating cancer. *Nature reviews. Clinical oncology* **12**, 527–540, https://doi.org/10.1038/nrclinonc.2015.120 (2015).
10. Bernier, J., Hall, E. J. & Giaccia, A. Radiation oncology: a century of achievements. *Nat Rev Cancer* **4**, 737–747, https://doi.org/10.1038/nrc1451 (2004).
11. Barker, H. E., Paget, J. T., Khan, A. A. & Harrington, K. J. The tumour microenvironment after radiotherapy: mechanisms of resistance and recurrence. *Nat Rev Cancer* **15**, 409–425, https://doi.org/10.1038/nrc3958 (2015).
12. Heckmann, M., Douwes, K., Peter, R. & Degitz, K. Vascular activation of adhesion molecule mRNA and cell surface expression by ionizing radiation. *Exp Cell Res* **238**, 148–154, https://doi.org/10.1006/excr.1997.3826 (1998).
13. Langley, R. E., Bump, E. A., Quartuccio, S. G., Medeiros, D. & Braunhut, S. J. Radiation-induced apoptosis in microvascular endothelial cells. *Br J Cancer* **75**, 666–672 (1997).
14. Garcia-Barros, M. *et al*. Tumor response to radiotherapy regulated by endothelial cell apoptosis. *Science* **300**, 1155–1159, https://doi.org/10.1126/science.1082504 (2003).
15. Gupta, A. *et al*. Radiotherapy promotes tumor-specific effector CD8+ T cells via dendritic cell activation. *J Immunol* **189**, 558–566, https://doi.org/10.4049/jimmunol.1200563 (2012).
16. Krysko, D. V. *et al*. Immunogenic cell death and DAMPs in cancer therapy. *Nature reviews. Cancer* **12**, 860–875, https://doi.org/10.1038/nrc3380 (2012).
17. Mao, A., Liu, Y., Zhang, H., Di, C. & Sun, C. microRNA expression and biogenesis in cellular response to ionizing radiation. *DNA and cell biology* **33**, 667–679, https://doi.org/10.1089/dna.2014.2401 (2014).
18. Kraemer, A. *et al*. MicroRNA-mediated processes are essential for the cellular radiation response. *Radiat Res* **176**, 575–586 (2011).
19. Czochor, J. R. & Glazer, P. M. microRNAs in cancer cell response to ionizing radiation. *Antioxid Redox Signal* **21**, 293–312, https://doi.org/10.1089/ars.2013.5718 (2014).
20. Gandellini, P., Rancati, T., Valdagni, R. & Zaffaroni, N. miRNAs in tumor radiation response: bystanders or participants? *Trends Mol Med* **20**, 529–539, https://doi.org/10.1016/j.molmed.2014.07.004 (2014).
21. Metheetrairut, C. & Slack, F. J. MicroRNAs in the ionizing radiation response and in radiotherapy. *Curr Opin Genet Dev* **23**, 12–19, https://doi.org/10.1016/j.gde.2013.01.002 (2013).
22. Wright, C. M., Dan, T., Dicker, A. P. & Simone, N. L. microRNAs: The Short Link between Cancer and RT-Induced DNA Damage Response. *Front Oncol* **4**, 133, https://doi.org/10.3389/fonc.2014.00133 (2014).
23. Kelley, K. A. *et al*. Understanding and Resetting Radiation Sensitivity in Rectal Cancer. *Annals of Surgery* **266**, 610–616, https://doi.org/10.1097/sla.0000000000002409 (2017).
24. Wilson, R. *et al*. MicroRNA regulation of endothelial TREX1 reprograms the tumour microenvironment. *Nature Communications* **7**, 13597, https://doi.org/10.1038/ncomms13597 (2016).
25. Liu, X.-F. *et al*. MiR-15a contributes abnormal immune response in myasthenia gravis by targeting CXCL10. *Clinical Immunology* **164**, 106–113, https://doi.org/10.1016/j.clim.2015.12.009 (2016).
26. Moon, H.-G., Yang, J., Zheng, Y. & Jin, Y. miR-15a/16 Regulates Macrophage Phagocytosis after Bacterial Infection. *The Journal of Immunology* **193**, 4558–4567, https://doi.org/10.4049/jimmunol.1401372 (2014).
27. Anand, S. *et al*. MicroRNA-132-mediated loss of p120RasGAP activates the endothelium to facilitate pathological angiogenesis. *Nat Med* **16**, 909–914, https://doi.org/10.1038/nm.2186 (2010).
28. Espinosa-Diez, C. *et al*. MicroRNA regulation of the MRN complex impacts DNA damage, cellular senescence, and angiogenic signaling. *Cell Death Dis* **9**, 632, https://doi.org/10.1038/s41419-018-0690-y (2018).
29. Ruhl, R. *et al*. microRNA-451a regulates colorectal cancer proliferation in response to radiation. *BMC Cancer* **18**, 517, https://doi.org/10.1186/s12885-018-4370-1 (2018).
30. Wang, Q. *et al*. Dual Anti-Inflammatory and Anti-Angiogenic Action of miR-15a in Diabetic Retinopathy. *EBioMedicine* **11**, 138–150, https://doi.org/10.1016/j.ebiom.2016.08.013 (2016).
31. De Meerleer, G. *et al*. Radiotherapy for renal-cell carcinoma. *The Lancet Oncology* **15**, e170–e177, https://doi.org/10.1016/s1470-2045(13)70569-2 (2014).
32. Kovacs, S. B. & Miao, E. A. Gasdermins: Effectors of Pyroptosis. *Trends in Cell Biology* **27**, 673–684, https://doi.org/10.1016/j.tcb.2017.05.005.
33. Kolb, J. P., Oguin, T. H., III, Oberst, A. & Martinez, J. Programmed Cell Death and Inflammation: Winter Is Coming. *Trends in Immunology* **38**, 705–718, https://doi.org/10.1016/j.it.2017.06.009.
34. Taabazuing, C. Y., Okondo, M. C. & Bachovchin, D. A. Pyroptosis and Apoptosis Pathways Engage in Bidirectional Crosstalk in Monocytes and Macrophages. *Cell chemical biology* **24**, 507–514.e504, https://doi.org/10.1016/j.chembiol.2017.03.009 Epub 2017 Apr 6. (2017).
35. Zhu, H. *et al*. The Effects of ASMase Mediated Endothelial Cell Apoptosis in Multiple Hypofractionated Irradiations in CT26 Tumor Bearing Mice. *Asian Pac J Cancer Prev* **16**, 4543–4548 (2015).
36. Ye, E.-A. *et al*. miR-15a/16 reduces retinal leukostasis through decreased pro-inflammatory signaling. *Journal of Neuroinflammation* **13**, https://doi.org/10.1186/s12974-016-0771-8 (2016).
37. Yang, J. *et al*. MiR-15a/16 deficiency enhances anti-tumor immunity of glioma-infiltrating CD8+ T cells through targeting mTOR. *International Journal of Cancer* **141**, 2082–2092, https://doi.org/10.1002/ijc.30912 (2017).
38. Lan, F. *et al*. miR-15a/16 Enhances Radiation Sensitivity of Non-Small Cell Lung Cancer Cells by Targeting the TLR1/NF-κB Signaling Pathway. *International Journal of Radiation Oncology*Biology*Physics* **91**, https://doi.org/10.1016/j.ijrobp.2014.09.021 (2015).
39. Mei, Z. *et al*. The miR-15 Family Enhances the Radiosensitivity of Breast Cancer Cells by Targeting G2 Checkpoints. *Radiation Research* **183**, https://doi.org/10.1667/rr13784.1 (2015).
40. Kontos, C. K., Tsiakanikas, P., Avgeris, M., Papadopoulos, I. N. & Scorilas, A. miR-15a-5p, A Novel Prognostic Biomarker, Predicting Recurrent Colorectal Adenocarcinoma. *Mol Diagn Ther* **21**, 453–464, https://doi.org/10.1007/s40291-017-0270-3 (2017).
41. Svoronos, A. A., Engelman, D. M. & Slack, F. J. OncomiR or Tumor Suppressor? The Duplicity of MicroRNAs in Cancer. *Cancer Research* **76**, 3666–3670, https://doi.org/10.1158/0008-5472.can-16-0359 (2016).

Acknowledgements

We thank Dr. Liana Tsikitis (OHSU) for useful discussions. We thank Drs Daniel G Anderson and Omar F. Khan (MIT) for 7C1 nanoparticles. We thank LaTroy Robinson for technical help. We acknowledge the OHSU Advanced Light Microscopy Core, Knight Cancer Institute Flow Cytometry Core and the Gene Profiling Shared Resource for technical help and useful discussions. This work was supported by US NIH grant R01HL137779 and R01HL143803 to S.A and a seed grant from ASTRO (Grant ID 534775) and RSNA to S.R.

Author contributions

S.R. and S.A. designed the study. S.R., C.E.D., N.C., C.H., E.F.B., A.A., S.K., R.R. performed the experiments, analyzed the data. S.R., S.A., C.R.T. analyzed and interpreted the data, drafted the manuscript. All authors reviewed the manuscript.

Competing interests

Dr. Anand receives grant funding from NIH, American Heart Association and institutional funds. Dr. Rana receives grant funding from American Society for Radiation Oncology (ASTRO) and Radiological Society of North America. Drs Anand, Thomas and Rana are named inventors on a provisional US patent application. Drs. Espinosa-Diez, Chatterjee, Fraile-Bethencourt, Agarwal, Khou and Ms Ruhl and Mr Hudson declare no conflict of interest.

Additional information

Supplementary information is available for this paper at https://doi.org/10.1038/s41598-020-62621-8.

Correspondence and requests for materials should be addressed to S.A.

Reprints and permissions information is available at www.nature.com/reprints.

Publisher's note Springer Nature remains neutral with regard to jurisdictional claims in published maps and institutional affiliations.